Crystal Structure of the Eukaryotic 40S Ribosomal Subunit in Complex with Initiation Factor 1

Julius Rabl, *et al.*

Science **331**, 730 (2011);
DOI: 10.1126/science.1198308

Crystal Structure of the Eukaryotic 40*S* Ribosomal Subunit in Complex with Initiation Factor 1

Julius Rabl,* Marc Leibundgut,* Sandro F. Ataide, Andrea Haag, Nenad Ban†

Eukaryotic ribosomes are substantially larger and more complex than their bacterial counterparts. Although their core function is conserved, bacterial and eukaryotic protein synthesis differ considerably at the level of initiation. The eukaryotic small ribosomal subunit (40*S*) plays a central role in this process; it binds initiation factors that facilitate scanning of messenger RNAs and initiation of protein synthesis. We have determined the crystal structure of the *Tetrahymena thermophila* 40*S* ribosomal subunit in complex with eukaryotic initiation factor 1 (eIF1) at a resolution of 3.9 angstroms. The structure reveals the fold of the entire 18*S* ribosomal RNA and of all ribosomal proteins of the 40*S* subunit, and defines the interactions with eIF1. It provides insights into the eukaryotic-specific aspects of protein synthesis, including the function of eIF1 as well as signaling and regulation mediated by the ribosomal proteins RACK1 and rpS6e.

Ribosomes are large cellular ribonucleoprotein assemblies responsible for protein synthesis in all organisms. Bacterial ribosomes consist of two subunits with a combined molecular weight of ~2600 kD. The small ribosomal subunit is responsible for decoding the information encoded in mRNA, whereas peptide bond synthesis occurs at the large ribosomal subunit (*1*). Although the core ribosomal function is preserved in all kingdoms of life, eukaryotic ribosomes are larger, ~4300 kD, and substantially more complex, comprising 45 additional proteins and two additional rRNAs (*2*, *3*). Although bacterial ribosome structure and function is well understood, thanks largely to experiments guided by atomic structures (*1*), many aspects of eukaryotic ribosome function have remained elusive. In contrast to bacterial systems, which require only three factors for translation initiation (*4*), the initiation of protein synthesis in eukaryotes involves at least 12 factors that assemble at the small ribosomal subunit in a highly regulated manner (*5*). Initiation of protein synthesis in eukaryotes is the target of regulation in a number of cellular processes including development, differentiation, stress response, and neuronal function (*6*); many diseases, including cancer and metabolic disorders, are connected with improper functioning or regulation of translation initiation (*7*). Furthermore, unlike in bacteria, the assembly and maturation pathway of eukaryotic ribosomes involves different compartments of the eukaryotic cell (*8*).

The structural understanding of eukaryotic ribosomes is currently limited to cryoelectron microscopy (cryo-EM) reconstructions at resolutions of 5.5 to 8 Å (*3*, *9*–*13*) and to a partial interpretation of the crystallographic data from the 80*S* yeast ribosome (*14*). These studies allowed localization of several eukaryotic-specific proteins of the small subunit (rpS4e, rpS19e, rpS25e, rpS27e, rpS28e, and RACK1). However, the folds and positions of most eukaryotic-specific proteins remain unclear.

Many of the additional functions of eukaryotic ribosomes involve the small ribosomal subunit because of its critical role in translation initiation. Relative to the bacterial small ribosomal subunit (30*S*), the eukaryotic small ribosomal subunit (40*S*) is larger by almost 500 kD (*2*, *15*). It consists of 33 proteins, 18 of which do not have homologs in bacteria, and an 18*S* rRNA (versus the bacterial 16*S* rRNA) (*3*). Eukaryotic initiation requires assembly of initiation factors eIF1, eIF1A, eIF3, and the eIF2 ternary complex (eIF2–GTP–Met-tRNA$_i^{Met}$) with the 40*S* subunit to form the 43*S* pre-initiation complex. eIF1 is recruited early in the process, as it is required for the formation of the full pre-initiation complex and is involved in scanning and recognition of the start codon on the mRNA. Structural information is available for eIF1 alone from nuclear magnetic resonance experiments (*16*, *17*), but the only information about its binding to the 40*S* subunit comes from hydroxyl radical probing and low-resolution cryo-EM (*18*, *19*).

To gain insight into the functioning of the eukaryotic ribosome and the process of translation initiation in eukaryotes, we determined the crystal structure of the *T. thermophila* eukaryotic small ribosomal subunit in complex with eIF1. The structure defines the locations and the folds of all 33 eukaryotic ribosomal proteins. It reveals the fold of the 18*S* rRNA including all of its eukaryotic expansion segments (ESs) and the details of its interactions with ribosomal proteins. Furthermore, it provides information on proteins responsible for eukaryotic-specific ribosomal functions in signaling and regulation, such as rpS6e and RACK1; rpS6e is phosphorylated in yeast and humans and is a target of the mTOR (mammalian target of rapamycin) pathway (*20*, *21*). Finally, the interactions with the eIF1 provide a basis for understanding its functions during translation initiation and the role of mutations that affect start codon recognition.

Crystallization and structure determination. We cocrystallized the *Tetrahymena thermophila* 40*S* ribosomal subunit together with eIF1 and determined the structure of the complex at 3.9 Å resolution (*22*). Experimental electron density maps calculated at 3.9 Å resolution using a combination of low-resolution cluster phasing and eightfold multicrystal averaging permitted the building of an atomic model of the entire 18*S* rRNA and all proteins of the small ribosomal subunit (Fig. 1, A to C, and tables S1 and S2). The protein and RNA segments included in the atomic model are given in table S1, together with the GenBank accession numbers. The two 40*S* subunits in the asymmetric unit are packed against each other via their 60*S* binding faces (fig. S1A), with the initiation factor mediating a crystal contact (fig. S1B). At 3.9 Å resolution, the core areas and most expansions of the proteins and the RNA could be built with confidence on the basis of landmarks such as bulky side chains, zinc ions in zinc finger proteins, salt bridges and general chemical environment, separation of stacked bases and the phosphate backbone, and secondary structure prediction (figs. S2 to S4) (*22*). However, the exact protein side chain conformations could not be determined at this resolution. Furthermore, we have also included in the model some intrinsically flexible solvent-exposed stretches of RNA and proteins, indicated by increased temperature factors (fig. S5), for which the sequence register is less reliable because it was established by extrapolation from the last identifiable residue. The final model could be refined to working and free *R* factors of 20.7% and 24.3%, respectively, with good geometry (table S2).

The structure of the *18S* rRNA. The structure of the eukaryotic 40*S* subunit can be divided into the traditional hallmark features of the small ribosomal subunit, comprising head, platform, body, beak, shoulder, right foot, and left foot. These are primarily defined by the fold of the 18*S* rRNA (Fig. 1A), which is composed of a region homologous to the prokaryotic 16*S* rRNA (Fig. 1B and fig. S6) with several eukaryotic-specific ESs (*23*). All ESs are visible in the structure and, except for the region interacting with rpS6e, reside on the surface of the 40*S* subunit. Helical elements of the ESs display variable lengths among eukaryotes; however, their basic architecture, as observed in this structure, is likely to be preserved. The two segments of ES3 (termed A and B) are located on the 5′ domain, ES6 and ES7

Institute of Molecular Biology and Biophysics, ETH Zürich, Schafmattstrasse 20, 8093 Zürich, Switzerland.

*These authors contributed equally to this work.
†To whom correspondence should be addressed. E-mail: ban@mol.biol.ethz.ch

form insertions in the central domain, and ES9 and ES12 are found in the 3′ major and the 3′ minor domain of the 18*S* RNA, respectively (Fig. 1, A and B, and fig. S6).

The longest ES in the eukaryotic 18*S* rRNA, ES6, consists of ~250 nucleotides forming five helices that replace the bacterial helix 21 (h21). ES6 is inserted between h20 and h22 in the lower back region of the 40*S* body (Fig. 1, A and B, and fig. S6). Helices A, B, C, and D form a large portion of the back of the 40*S* body (Fig. 1D), and their structure differs considerably from a previous model (*3*). Helices C and D are located at an equivalent position to bacterial h21. They stretch across the back of 40*S* and are buried underneath helix A. The apical loop region of ES6B is exposed and disordered in the structure, making it prone to chemical modification and cleavage by nucleases, as previously observed (*24*). The loop region of helix ES6E forms a base pair with ES3B, yielding an extended helix that projects from the center of the back toward the left foot of the 40*S* (Fig. 1D and fig. S6). This somewhat unusual quaternary interaction was demonstrated earlier by computational and biochemical experiments (*24*). The ES3B apical region packs against ES3A to form the left foot along with ES6E. The quaternary interaction of the eukaryotic ES3 and ES6, together with several proteins, forms a new domain responsible for the broader back and more prominent left foot features of the 40*S* (Fig. 1, A and D, and table S3).

Helix h16, which is situated directly below the beak, is shifted relative to the position in bacteria by as much as 40 Å (Fig. 1E). The position of h16 in the 40*S* crystal structure is consistent with those observed in solution by cryo-EM of the empty yeast 40*S*, the 40*S*-eIF1 or 40*S*-eIF1A complex (*19*), and canine and *Thermomyces lanuginosus* 80*S* (*3*, *9*). h16 is involved in forming a connection between the head and the body of the 40*S* subunit upon binding of initiation factors eIF1 and eIF1A, which might point to a role of this helix in initiation (*19*).

Ribosomal proteins. The structure of the eukaryotic 40*S* subunit contains 33 proteins, 18 of which are absent in bacteria (Fig. 1C, Fig. 2, fig. S7, and table S4) (*22*). In addition, more than half of the conserved ribosomal proteins contain eukaryotic-specific extensions. Three of the eukaryotic ribosomal proteins are positional analogs that have replaced bacterial 30*S* proteins: Bacterial rpS6p and rpS18p at the platform are replaced by rpS1e (fig. S7G), whereas bacterial

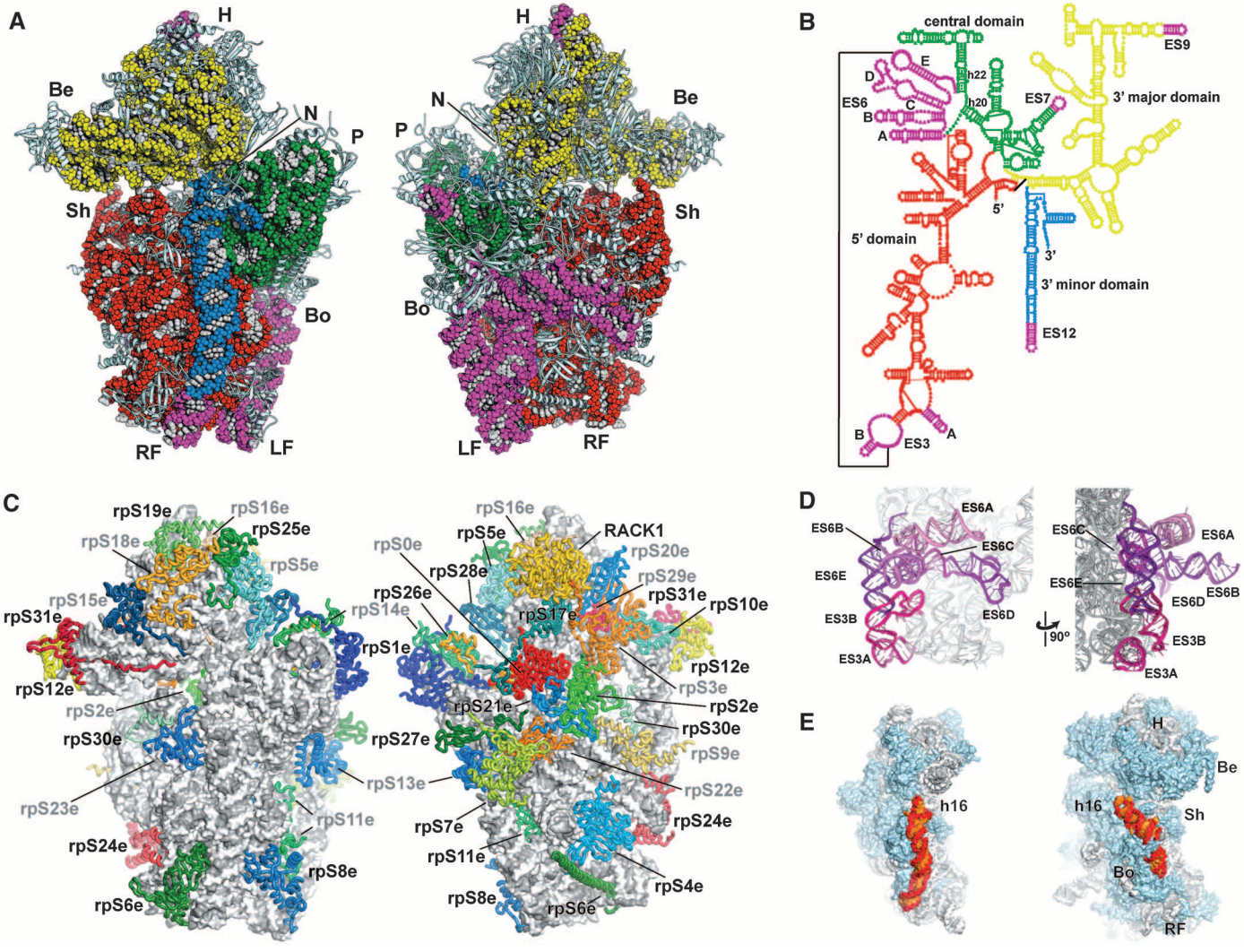

Fig. 1. Architecture of the 40*S*. (**A**) Front and back views of the tertiary structure of the 40*S* showing the 18*S* rRNA as spheres and colored according to each domain (5′ domain, red; central domain, green; 3′ major domain, yellow; 3′ minor domain, blue; ESs, magenta), and the proteins as gray cartoons (abbreviations: H, head; Be, beak; N, neck; P, platform; Sh, shoulder; Bo, body; RF, right foot; LF, left foot). (**B**) Secondary structure diagram of the *T. thermophila* 18*S* RNA (modified from www.rna.ccbb.utexas.edu) showing the rRNA domains and the locations of the ESs. (**C**) Ribosomal proteins of the 40*S* are shown as cartoons in individual colors; rRNA is shown as gray surface. The 40*S* is shown in front and back view, in the same orientation as in (A). (**D**) View of the quaternary interactions between ES6 and ES3 at the back of the 40*S*. The RNA is displayed as a cartoon with the proteins omitted for clarity. ES6 helices are colored in a gradient from light to dark magenta and labeled from A to E, following the nomenclature of (*24*). ES3 is highlighted in pink, and the rest of the 18*S* rRNA is colored in gray. (**E**) The position of helix h16 in bacterial 30*S* [left, drawn from (*35*)] and in 40*S*.

rpS16p at the foot has been substituted by rpS4e. Eukaryotic ribosomal protein rpS30e occupies a similar space as bacterial rpS4p, but unlike rpS4p it extends into the intersubunit interface (fig. S7I).

The feet of the bacterial ribosome are extensively remodeled in eukaryotes, where h9, ES3, and ES6E of the 18*S* rRNA and eukaryotic ribosomal proteins rpS4e, rpS6e, and rpS8e have replaced bacterial rpS20p (Fig. 1C and Fig. 2).

The beak of the eukaryotic ribosome has transformed from an all-rRNA structure to a protein protuberance in eukaryotes: Eukaryotic ribosomal proteins rpS10e, rpS12e [a structural analog of archaeal large ribosomal subunit protein rpL7Ae (fig. S7F) (*25*)], and rpS31e are bound to a reduced h33 of the 18*S* rRNA, giving the eukaryotic protein beak essentially the same conserved shape as observed for the bacterial 30*S* subunit (Fig. 3A). rpS31e, which is expressed as a ubiquitin fusion protein (*26*), stretches from the A-site close to the decoding center toward the beak, where its zinc finger motif is located (Fig. 3B and fig. S8). Failure to cleave the N-terminal ubiquitin domain would result in a 40*S* subunit that cannot engage in initiation because of the steric hindrance of the decoding center by the attached domain. Indeed, mutations that prevent cleavage of the ubiquitin moiety from rpS31e are lethal in yeast (*27*).

The additional eukaryotic-specific proteins, which are mostly located at the back of the small subunit, contact the 18*S* rRNA, bind to each other, or interact with conserved ribosomal proteins (Fig. 1C, Fig. 2, and fig. S9). In contrast, eukaryotic-specific extensions of conserved proteins are found clustering and interacting primarily with eukaryotic-specific proteins (Fig. 2 and fig. S9).

In bacteria, five of 20 ribosomal proteins interact with no other ribosomal protein. By con-

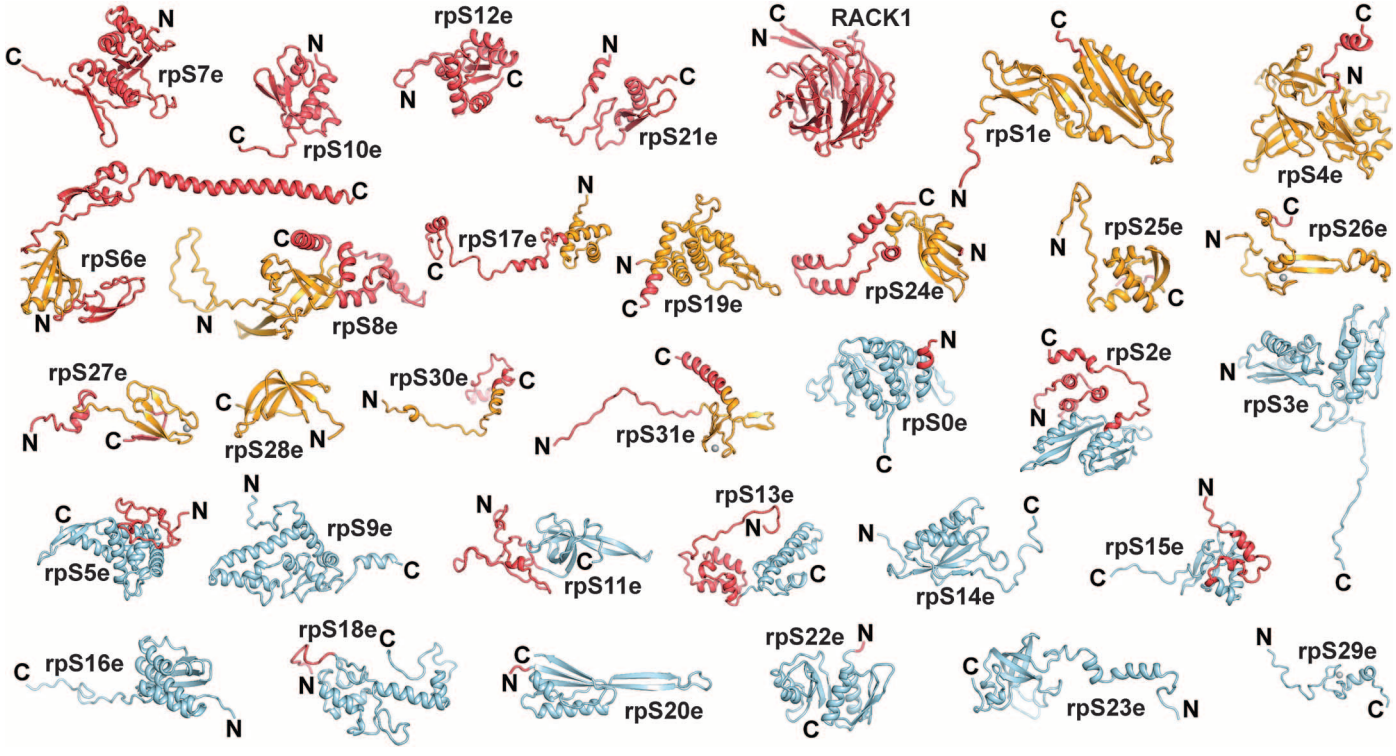

Fig. 2. Fold and conservation of all ribosomal proteins of the 40*S* subunit. Backbones of all ribosomal proteins are shown colored according to the distribution across kingdoms of life; positions of the N and C termini are indicated. Protein cores found in all kingdoms are presented in light blue; archaeal cores are depicted in orange. Proteins or extensions uniquely found in eukaryotes are depicted in red.

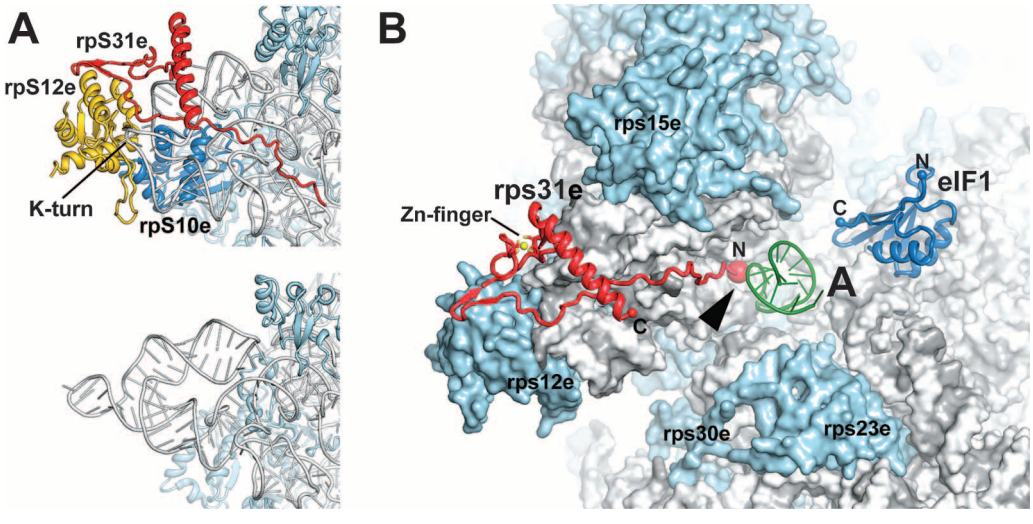

Fig. 3. Remodeling of the beak region of the eukaryotic ribosome through reduction of rRNA and addition of proteins. (**A**) The rRNA at the beak is reduced in *T. thermophila* and instead contains a kink-turn motif to which rpS12e is bound. Further beak areas are substituted by rpS10e and rpS31e. The bacterial beak structure of *T. thermophilus* shown below is predominantly formed by rRNA (*35*). (**B**) Position of the ubiquitin fusion protein rpS31e with relation to the A-site and initiation factor eIF1. The N terminus of rpS31e is seen stretching toward the A-site. An arrow indicates the position where the uncleaved ubiquitin domain would be located. Part of a tRNA modeled into the A-site according to Selmer *et al.* (*53*) is shown in green. eIF1 is shown in blue.

trast, all ribosomal proteins of the *T. thermophila* 40*S* subunit contact at least one other ribosomal protein (table S5), and the total interaction surface between ribosomal proteins in the 40*S* subunit is almost four times the 30*S* ribosomal protein-protein interaction surface (40*S*, ~25,000 Å^2; 30*S*, ~6500 Å^2) (table S5). Although the increased number of ribosomal proteins in the 40*S* is partly responsible for the larger interaction surface, the average interaction surface of a eukaryotic protein is nonetheless larger than a bacterial protein in the 30*S* subunit by a factor of 2.4. For example, ribosomal protein rpS21e, although rather small, has large contact surfaces with three other ribosomal proteins (rpS0e, rpS2e, and rpS22e) with a total interaction surface of more than 3400 Å^2, whereas it makes only very limited contact with the 18*S* rRNA (fig. S10). Long extended C- or N-terminal regions of proteins, frequently involved in RNA interactions in bacteria, are occasionally found to be responsible for large distance-bridging contacts between eukaryotic proteins in the 40*S* subunit. For example, the C terminus of rpS3e stretches from the core of rpS3e near the beak toward RACK1, while the C terminus of rpS17e meanders away from RACK1 along the back of the ribosome over a distance of at least 48 Å, where it binds to rpS0e (Fig. 1C).

Positioning of all ribosomal proteins of the 40*S* subunit allows rationalization of biochemical and genetic data on ribosome biogenesis and human diseases such as Diamond-Blackfan anemia and 5q− syndrome. Although the distribution of ribosomal proteins shows a striking correlation with the biochemical and genetic data regarding their involvement in different stages of ribosome biogenesis (fig. S11) (*22*), ribosomal proteins associated with human disorders are scattered all over the 40*S* subunit (fig. S12) (*22*). The latter suggests that these mutations perturb ribosome stability or assembly rather than affecting a specific function of the 40*S* subunit.

The mRNA interacting channel of the 40*S* subunit. To overcome steric hindrance by mRNA secondary structure elements during translation, the ribosome depends on an intrinsic helicase activity that unwinds the mRNA (*28*). In bacteria, three basic residues of rpS3p, which is located at the head, and two basic residues of rpS4p, which is located at the body, protrude into the mRNA channel (Fig. 4A) and interact with the phosphate backbone of the mRNA secondary structure,

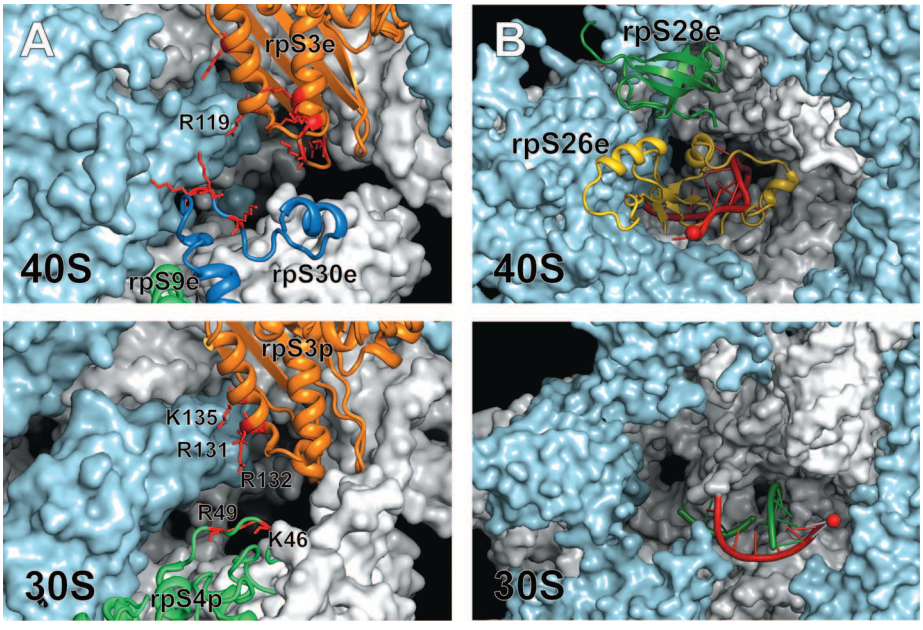

Fig. 4. The mRNA path through the eukaryotic ribosome. (**A**) Basic residues are found extending from ribosomal proteins at the head and shoulder of 40*S* into the mRNA channel. The bacterial 30*S* is drawn below for comparison in the same orientation as 40*S*. Basic residues responsible for helicase function of bacterial ribosomes [drawn from (*28*, *35*)] are shown in red. (**B**) The region surrounding the 3′ end of the rRNA differs between bacteria and eukaryotes. The 3′ end of the 16*S* rRNA in bacteria (lower panel, red) is flexible and able to form base pairs with Shine-Dalgarno oligonucleotide mimics [green, drawn from (*30*)], whereas the 3′ end of 18*S* rRNA (upper panel, red) is locked in place by rpS26e (yellow). The fold of rpS28e (green) is related to that of bacterial rpS1p.

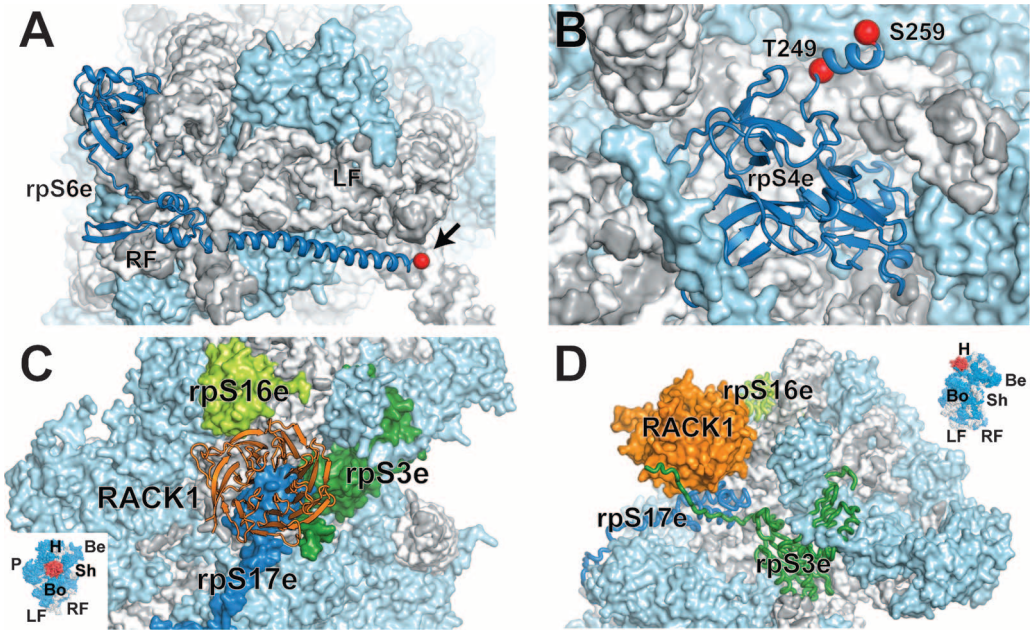

Fig. 5. Regulatory proteins of the 40*S* subunit. (**A**) The region in which rpS6e (dark blue) of most eukaryotes is phosphorylated is disordered in the crystal structure. It is located directly behind the last ordered C-terminal residue (arrow, red sphere). (**B**) The phosphorylation sites Thr^{249} and Ser^{259} (red spheres) of *T. thermophila* rpS4e are located near the C terminus. (**C**) Top view of RACK1 at the ribosome. 18*S* rRNA is shown in surface representation in gray; proteins not involved in RACK1 binding are shown in surface representation in light blue. Proteins rpS3e, rpS16e, and rpS17e, which were found to interact with RACK1, are shown in dark green, light green, and blue, respectively. (**D**) Side view of RACK1 at the ribosome shows binding of the C terminus of rpS3e to RACK1. Proteins rpS3e, rpS16e, and rpS17e are shown in dark green, light green, and blue tube representation, respectively; RACK1 is shown as orange surface. Insets in (C) and (D) show the overall view of the 40*S* in the same orientation as the magnified images.

which is unfolded by movement of the head relative to the body (*28*, *29*). In eukaryotes, the mRNA channel has been extensively remodeled but still shows features that are compatible with helicase activity (Fig. 4A). Several basic residues of eukaryotic rpS3e (homolog to bacterial rpS3p) are oriented toward the mRNA channel, with the position of Arg^{119} conserved from bacteria to humans. The eukaryotic homolog of bacterial protein rpS4p, rpS9e, is shorter and does not extend to the mRNA channel. However, an extension of the eukaryotic-specific rpS30e has three basic residues oriented toward the mRNA channel and appears to serve as a partial positional and functional analog of bacterial rpS4p (Fig. 4A).

Translation initiation in bacteria depends on interactions of two regions of the small ribosomal subunit with the 5′ untranslated region of mRNA: the anti–Shine-Dalgarno sequence near the 3′ end of the 16*S* rRNA (*30*, *31*) and, in most bacteria, ribosomal protein rpS1p (*32*–*34*). Crystal structures of the 30*S* subunit lacking rpS1p with and without Shine-Dalgarno mimics (*30*, *35*) have shown flexibility of the 3′ end of the 16*S* rRNA, which is either found bound to the decoding center or folded back and base-paired to the Shine-Dalgarno mimics (Fig. 4B). Translation initiation in eukaryotes, however, requires neither an rpS1p homolog nor a Shine-Dalgarno sequence (*36*). In the structure of the 40*S*, the area corresponding to the bacterial Shine-Dalgarno chamber, where rpS1p has been visualized in EM studies of the 30*S* subunit (*33*), is partially occupied by the eukaryotic proteins rpS26e and rpS28e (Fig. 4B). The β-barrel structure of rpS28e is related to the structure of the RNA binding domain of rpS1p (fig. S13A) (*37*). In contrast to the flexible 3′ end of bacterial 16*S* rRNA, the 3′ end of the eukaryotic 18*S* rRNA appears to be locked in place by tight interactions with rpS26e (fig. S13B).

Regulation of signaling pathways by rpS4e, rpS6e, and RACK1. The crystal structure of *T. thermophila* 40*S* provides insights into signaling at the small ribosomal subunit. We focus in particular on rpS6e, a target of the mTOR pathway (*21*); rpS4e, which is specifically phosphorylated in *Tetrahymena* (*38*); and RACK1, a central cellular signaling hub at the ribosome (*39*).

Ribosomal protein rpS6e extends from the right to the left foot of the 40*S*. It is organized in two regions: The N-terminal β-barrel domain (residues 2 to 130), located at the right foot, is connected to a long C-terminal α helix (residues 186 to 224), which spans between h10 and ES6B at the left foot of the 40*S*, via a highly basic, partially folded linker (residues 131 to 185) that makes numerous connections to the rRNA phosphate backbone (Fig. 5A and fig. S7B). The C-terminal extension of 70 amino acids, which is unique to ciliates and follows the α helix, is disordered in our structure. Phosphorylation in response to mTOR signaling occurs at two serines in yeast, and at five serines in humans and other metazoans, at a conserved site near the C terminus (*21*) (fig. S14). Although rpS6e phosphorylation does not occur in *T. thermophila* (*38*) and serines conserved in yeast and metazoans are absent in *T. thermophila* rpS6e, the structure of *T. thermophila* rpS6e allows us to assign the approximate location of the phosphorylation sites. These sites are exposed and therefore accessible to the rpS6e kinase, which may use basic patches on its surface to bind rRNA (*40*). They are located at least 130 Å from the decoding center on the back of the small ribosomal subunit. This argues against a model in which phosphorylation of the conserved serines would directly influence protein translation by altering the interaction of rpS6e with initiation factors, mRNAs, or tRNAs (*41*) (fig. S15).

In *T. thermophila*, rpS4e is phosphorylated at residues Thr^{249} and Ser^{259} in response to starvation or exposure to sodium ions (*38*). Ribosomal protein rpS4e is located at the back of the ribosome and is firmly anchored within ES3, ES6, h7, and h15 of the 18*S* rRNA (Fig. 5B). The N terminus meanders into the interior of the rRNA core of the 40*S* but does not reach the subunit interface, while the majority of the protein folds into three subdomains on the surface of the 40*S* (fig. S7J) (*22*). Residues Thr^{249} and Ser^{259} are located at the C terminus of rpS4e and are solvent-exposed. Because there is limited evidence for rpS4e phosphorylation in organisms other than *Tetrahymena* (*38*) and because the penultimate serine is not conserved, the biological importance of rpS4e phosphorylation remains unclear.

RACK1 is a WD (Trp-Asp) repeat protein that serves as a signaling scaffold. It interacts with a multitude of cellular proteins and assemblies including the ribosome (*39*) and is recruited by viral proteins during infection (*42*–*45*). RACK1 has been identified as a core ribosomal protein of the small ribosomal subunit (*46*), which suggests a regulatory link between signaling and translation. In yeast, RACK1 is found associated with the ribosomal 40*S* subunit in actively growing cells and in the soluble fraction of stationary-phase cells (*47*). The structure of *T. thermophila* 40*S* contains bound RACK1 despite purification of the ribosomal subunit at high salt concentrations (700 mM KCl), consistent with previous experiments (*46*). RACK1 makes extensive contacts not only with the phosphate backbone and bases of h39 and h40 of 18*S* rRNA, but also with ribosomal proteins rpS16e, rpS17e, and rpS3e with a total contact surface of more than 1000 $Å^2$ (Fig. 5, C and D, and table S5). The interaction with rpS17e through several salt bridges is com-

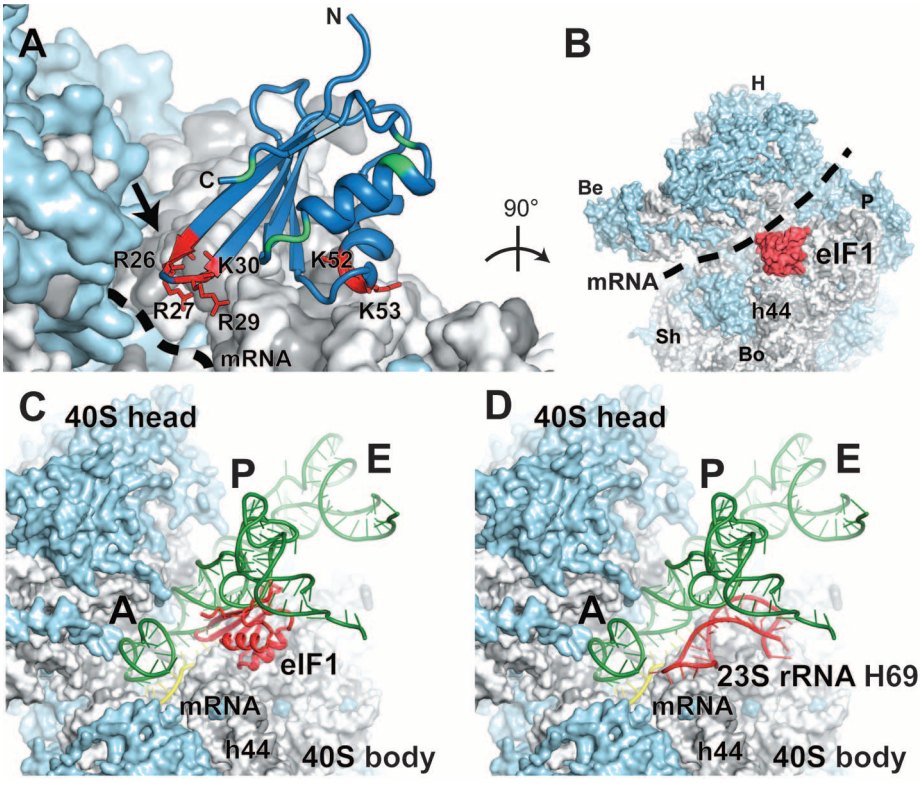

Fig. 6. Eukaryotic initiation factor eIF1 bound to the 40*S* subunit. (**A**) Eukaryotic initiation factor eIF1 binds to the 18*S* rRNA phosphate backbone (shown as gray surface) with basic residues (shown in red). The basic loop of eIF1 found in close proximity to the mRNA channel is indicated with an arrow. Genetic experiments implicate residues behind the basic loop, at the end of one of the helices and the penultimate residue in cognate codon recognition (green). (**B**) *T. thermophila* eIF1 (red) is located at the top of h44 below the platform. Dashed lines indicate the mRNA path on the 40*S* subunit. (**C** and **D**) Molecular modeling of A-, P-, and E-site tRNAs (green) and mRNA (yellow) shows the equivalent positioning of eIF1 in the initiation complex (C) and helix H69 of the 23*S* rRNA (red) in the translating 70*S* ribosome (D) (*53*).

parable to the RACK1 interactions with rRNA, whereas only a few residues of rpS16e are involved in contacts with RACK1. The C terminus of rpS3e is attached to blade 5 of RACK1 by at least two salt bridges (Fig. 5D). Given the extent and chemistry of the contacts between RACK1 and the ribosome, it is likely that they associate tightly and that, as proposed in (*39*), free RACK1 originates from RACK1 up-regulation rather than from release of RACK1 from ribosomes. The rRNA and ribosomal proteins obscure a large part of the RACK1 surface in the 40*S* structure, especially WD repeats 1, 2, and 5. Thus, inclusion into the 40*S* subunit may alter the properties of RACK1 in signaling. Indeed, two signaling protein binding sites in human RACK1—Tyr^{52} (Tyr^{64} in *T. thermophila*), the site of phosphorylation by c-Abl, and the binding sites of focal adhesion kinase (FAK) (*48*)—are at least partially occluded when RACK1 is bound to the ribosome (fig. S16); this may provide a structural explanation for the result of a recent study in yeast, which suggests a connection between the location of RACK1 at the ribosome and RACK1 function in signaling (*20*).

Initiation factor eIF1. The eukaryotic initiation factor eIF1 has no structural homolog in bacteria, although some aspects of its function are likely carried out by IF3 (*4*). The factor is involved with several crucial tasks during eukaryotic translation initiation: Cooperative binding of eIF1 and eIF1A induces the open, scanning-competent conformation in the 40*S* subunit (*19*, *49*). During scanning, eIF1 is able to recognize a start codon and dissociates from the initiation complex upon codon recognition, which induces the closed conformation in the 40*S* (*50*).

Although eIF1 contacts two 40*S* subunits in the crystal, only one of the interactions is extensive and likely to be functionally relevant (fig. S1) (*22*), given the agreement of our findings with the results of directed hydroxyl radical probing experiments of the 40*S*-eIF1 complex (*18*). eIF1 binds to the 40*S* subunit at the top of h44 and to h24 of the 18*S* rRNA, on the left side of the platform directly below the P-site, in a position that brings the basic loop (Arg^{26}-Lys^{30}) of the factor into close proximity to the mRNA channel (Fig. 6, A and B). Because eIF1 does not bridge the head and the body, it is unlikely that binding of eIF1 alone arrests the 40*S* subunit in a particular conformation. Indeed, the head of the 40*S* in different space groups is found in different conformations relative to the body, with displacements up to 6 Å (fig. S17). It is therefore possible that binding of eIF1A, whose helical subdomain has been found binding to the head of the 40*S* subunit by hydroxyl radical probing experiments (*51*), rather than eIF1, is primarily responsible for arresting the 40*S* subunit in the open, scanning-competent conformation. The position of eIF1A on the 40*S* subunit, which can be inferred by superimposing the bacterial homolog (IF1) bound to 30*S* ribosomal subunit onto the 40*S* subunit (*52*), would be directly adjacent to eIF1. On the basis of this model, it is likely that the two factors would directly contact each other with their core domains, which would explain the cooperative binding of the two factors (*49*) (fig. S18). However, further structural investigations will be necessary to learn the details of the putative eIF1-eIF1A interaction.

eIF1 contacts the rRNA backbone with three residues that are conserved from yeast to human: Arg^{29}, Lys^{52}, and Lys^{53} (in yeast, Arg^{36}, Lys^{59}, and Lys^{60}) at bases U1711, U982, and G1733, respectively (Fig. 6A). A conserved basic loop including residues 26 to 30 (residues 33 to 37 in yeast) extends into the mRNA channel, where it would be in direct proximity to mRNA and the anticodon stem loop of the tRNA in the P-site, as implicated by superimposing the bacterial 70*S*-mRNA-tRNA complex (*53*) onto the 40*S*-eIF1 complex (Fig. 6C). Interestingly, only one residue of the basic loop actually contacts the rRNA phosphate backbone (at U1711), whereas the other residues (Arg^{26}, Arg^{27}, and Lys^{30}) have less well defined side-chain densities and are free to interact with the content of the mRNA channel (Fig. 6A). These residues may detect cognate codon interactions in the mRNA channel and act as a sensor for structural changes induced by codon recognition. Although the details of how eIF1 communicates codon recognition are not clear, mutations in yeast eIF1 [suppressor of initiation codon mutations (sui^-)] that lead to recognition of near-cognate start codons (as a result of premature departure of eIF1 from the complex) implicate the second α helix and the penultimate residue of eIF1 in this process (*17*, *50*, *54*, *55*) (Fig. 6A). Additionally, the N-terminal tail of the eIF1 has been shown to play a role in eIF2–GTP–Met-$tRNA_i^{Met}$ (ternary complex) loading during translation initiation (*56*). In the crystal structure, the N-terminal extension is disordered and points away from the 40*S* subunit, where it may become available for interactions with the ternary complex (Fig. 6A and fig. S1B).

Structural superpositioning of the *T. thermophila* 40*S* ribosomal subunit with the bacterial 70*S* containing A-, P-, and E-site tRNAs [*T. thermophilus*, PDB IDs 2j02 and 2j03 (*53*)] reveals that eIF1 would sterically clash with the highly conserved helix H69 of the large-subunit rRNA and thus serve as an anti-association factor (Fig. 6, C and D, and fig. S19). Such a role has also been proposed for the C domain of bacterial IF3, which was mapped to a similar area on the small subunit on the basis of hydroxyl radical probing experiments (*57*). In the translating bacterial ribosome, the P-site tRNA is in close contact with helix H69 (Fig. 6D), whereas in the eukaryotic initiation complex during scanning, eIF1 together with the other initiation factors might contribute to stabilizing the initiator tRNA by serving as a binding platform (Fig. 6C), although the tRNA or eIF1 would have to be slightly repositioned because of mild steric clashes, either. The tRNA-eIF1 interaction surface suggested by the superimposed models is further corroborated by hydroxyl radical cleavage patterns on the initiator tRNA observed in 43*S* preinitiation complexes (*18*). In these studies, hydroxyl radicals generated from Fe(II) attached to exposed eIF1 residues lead to initiator tRNA cleavage in the A and D stems at locations compatible with our model (fig. S20).

Note that the surface potential of eIF1 is strongly positive on the side facing toward the 40*S* rRNA, whereas the face oriented toward the P-site tRNA shows a more heterogeneous charge distribution, indicating that the tRNA contact would be mediated mainly via hydrophobic residues and by only a few positively charged residues (fig. S20).

Conclusions. The crystal structure of the 40*S* subunit provides insights into the evolution of eukaryotic ribosomes and into their eukaryotic-specific functions. The structure also reveals interactions of the 40*S* subunit with eIF1 as a first step toward understanding eukaryotic translation initiation. Structure-based biochemical and genetic experiments and additional crystallographic studies of the system described here will enable further investigation of many remaining questions regarding the assembly, maturation, and nuclear export of the 40*S* subunit and its role in the regulation of translation initiation.

References and Notes

1. T. M. Schmeing, V. Ramakrishnan, *Nature* **461**, 1234 (2009).
2. J. Dresios, P. Panopoulos, D. Synetos, *Mol. Microbiol.* **59**, 1651 (2006).
3. D. J. Taylor *et al.*, *Structure* **17**, 1591 (2009).
4. B. S. Laursen, H. P. Sørensen, K. K. Mortensen, H. U. Sperling-Petersen, *Microbiol. Mol. Biol. Rev.* **69**, 101 (2005).
5. R. J. Jackson, C. U. Hellen, T. V. Pestova, *Nat. Rev. Mol. Cell Biol.* **11**, 113 (2010).
6. N. Sonenberg, A. G. Hinnebusch, *Cell* **136**, 731 (2009).
7. D. Silvera, S. C. Formenti, R. J. Schneider, *Nat. Rev. Cancer* **10**, 254 (2010).
8. I. Zemp, U. Kutay, *FEBS Lett.* **581**, 2783 (2007).
9. P. Chandramouli *et al.*, *Structure* **16**, 535 (2008).
10. T. Becker *et al.*, *Science* **326**, 1369 (2009); 10.1126/science.1178535.
11. S. Bhushan *et al.*, *Nat. Struct. Mol. Biol.* **17**, 313 (2010).
12. J. P. Armache *et al.*, *Proc. Natl. Acad. Sci. U.S.A.* **107**, 19748 (2010).
13. J. P. Armache *et al.*, *Proc. Natl. Acad. Sci. U.S.A.* **107**, 19754 (2010).
14. A. Ben-Shem, L. Jenner, G. Yusupova, M. Yusupov, *Science* **330**, 1203 (2010).
15. W. M. Clemons Jr. *et al.*, *Nature* **400**, 833 (1999).
16. C. M. Fletcher, T. V. Pestova, C. U. Hellen, G. Wagner, *EMBO J.* **18**, 2631 (1999).
17. M. Reibarkh *et al.*, *J. Biol. Chem.* **283**, 1094 (2008).
18. I. B. Lomakin, V. G. Kolupaeva, A. Marintchev, G. Wagner, T. V. Pestova, *Genes Dev.* **17**, 2786 (2003).
19. L. A. Passmore *et al.*, *Mol. Cell* **26**, 41 (2007).
20. S. M. Coyle, W. V. Gilbert, J. A. Doudna, *Mol. Cell. Biol.* **29**, 1626 (2009).
21. O. Meyuhas, *Int. Rev. Cell Mol. Biol.* **268**, 1 (2008).
22. See supporting material on *Science* Online.
23. J. J. Cannone *et al.*, *BMC Bioinformatics* **3**, 2 (2002).
24. G. Alkemar, O. Nygård, *Biochemistry* **45**, 8067 (2006).
25. K. Ye *et al.*, *Proc. Natl. Acad. Sci. U.S.A.* **106**, 13808 (2009).
26. K. L. Redman, M. Rechsteiner, *Nature* **338**, 438 (1989).
27. T. Lacombe *et al.*, *Mol. Microbiol.* **72**, 69 (2009).
28. S. Takyar, R. P. Hickerson, H. F. Noller, *Cell* **120**, 49 (2005).
29. M. A. Borovinskaya, S. Shoji, J. M. Holton, K. Fredrick, J. H. Cate, *ACS Chem. Biol.* **2**, 545 (2007).

30. T. Kaminishi *et al.*, *Structure* **15**, 289 (2007).
31. A. Korostelev *et al.*, *Proc. Natl. Acad. Sci. U.S.A.* **104**, 16840 (2007).
32. A. V. Komarova, L. S. Tchufistova, E. V. Supina, I. V. Boni, *RNA* **8**, 1137 (2002).
33. J. Sengupta, R. K. Agrawal, J. Frank, *Proc. Natl. Acad. Sci. U.S.A.* **98**, 11991 (2001).
34. M. A. Sørensen, J. Fricke, S. Pedersen, *J. Mol. Biol.* **280**, 561 (1998).
35. B. T. Wimberly *et al.*, *Nature* **407**, 327 (2000).
36. L. D. Kapp, J. R. Lorsch, *Annu. Rev. Biochem.* **73**, 657 (2004).
37. M. Bycroft, T. J. P. Hubbard, M. Proctor, S. M. V. Freund, A. G. Murzin, *Cell* **88**, 235 (1997).
38. L. Palm *et al.*, *J. Biol. Chem.* **270**, 6000 (1995).
39. J. Nilsson, J. Sengupta, J. Frank, P. Nissen, *EMBO Rep.* **5**, 1137 (2004).
40. T. Sunami *et al.*, *J. Biol. Chem.* **285**, 4587 (2010).
41. K. Pachler *et al.*, *FEMS Yeast Res.* **5**, 271 (2004).
42. N. Sang *et al.*, *J. Biol. Chem.* **276**, 27026 (2001).
43. A. Gallina, F. Rossi, G. Milanesi, *Virology* **283**, 7 (2001).
44. P. R. Smith *et al.*, *J. Virol.* **74**, 3082 (2000).
45. J. Reinhardt, T. Wolff, *Vet. Microbiol.* **74**, 87 (2000).
46. A. J. Link *et al.*, *Nat. Biotechnol.* **17**, 676 (1999).
47. S. Baum, M. Bittins, S. Frey, M. Seedorf, *Biochem. J.* **380**, 823 (2004).
48. P. A. Kiely *et al.*, *J. Biol. Chem.* **284**, 20263 (2009).
49. D. Maag, J. R. Lorsch, *J. Mol. Biol.* **330**, 917 (2003).
50. J. S. Nanda *et al.*, *J. Mol. Biol.* **394**, 268 (2009).
51. Y. Yu *et al.*, *Nucleic Acids Res.* **37**, 5167 (2009).
52. A. P. Carter *et al.*, *Science* **291**, 498 (2001); 10.1126/science.1057766.
53. M. Selmer *et al.*, *Science* **313**, 1935 (2006); 10.1126/science.1131127.
54. B. Castilho-Valavicius, H. Yoon, T. F. Donahue, *Genetics* **124**, 483 (1990).
55. H. J. Yoon, T. F. Donahue, *Mol. Cell. Biol.* **12**, 248 (1992).
56. Y. N. Cheung *et al.*, *Genes Dev.* **21**, 1217 (2007).
57. A. Dallas, H. F. Noller, *Mol. Cell* **8**, 855 (2001).
58. All data were collected at the Swiss Light Source (SLS, Paul Scherrer Institut, Villigen). We thank C. Schulze-Briese, A. Pauluhn, R. Bingel-Erlenmeyer, M. Müller, and T. Tomizaki for their outstanding support at the SLS; B. Blattmann from the NCCR crystallization facility for screening; R. Brunisholz for help with mass spectroscopy; N. Katheder, D. Baretic, and M. Weisser for their work during the initial phase of the project; S. Arpagaus for preparation of the material; T. Maier for advice during phasing; D. Böhringer for critically reading the manuscript; all members of the Ban laboratory for suggestions and discussions; and A. Brünger for providing a prerelease version of the CNS 1.3 refinement program. Supported by the Swiss National Science Foundation (SNSF), the National Center of Excellence in Research (NCCR) Structural Biology program of the SNSF, and European Research Council grant 250071 under the European Community's Seventh Framework Programme (N.B.), and the Max Roessler prize to N.B. Coordinates and structure factors have been deposited in the Protein Data Bank (PDB) with accession codes 2xzm and 2xzn. ETH Zürich has filed a patent application to use the crystals and the coordinates of the 40*S* ribosomal subunit for developing compounds that can interfere with eukaryotic translation.

Supporting Online Material

www.sciencemag.org/cgi/content/full/science.1198308/DC1
Materials and Methods
SOM Text
Figs. S1 to S20
Tables S1 to S6
References

27 September 2010; accepted 15 December 2010
Published online 23 December 2010;
10.1126/science.1198308

REPORTS

Discovery of Powerful Gamma-Ray Flares from the Crab Nebula

M. Tavani,[1,2,3,4]* A. Bulgarelli,[5] V. Vittorini,[1] A. Pellizzoni,[16] E. Striani,[2,4] P. Caraveo,[7] M. C. Weisskopf,[21] A. Tennant,[21] G. Pucella,[6] A. Trois,[1] E. Costa,[1] Y. Evangelista,[1] C. Pittori,[19] F. Verrecchia,[19] E. Del Monte,[1] R. Campana,[1] M. Pilia,[16,17] A. De Luca,[7,25] I. Donnarumma,[1] D. Horns,[22] C. Ferrigno,[23] C. O. Heinke,[24] M. Trifoglio,[5] F. Gianotti,[5] S. Vercellone,[18] A. Argan,[1] G. Barbiellini,[3,8,9] P. W. Cattaneo,[10] A. W. Chen,[3,7] T. Contessi,[7] F. D'Ammando,[18] G. DeParis,[1] G. Di Cocco,[5] G. Di Persio,[1] M. Feroci,[1] A. Ferrari,[3,11] M. Galli,[12] A. Giuliani,[7] M. Giusti,[1,3] C. Labanti,[5] I. Lapshov,[13] F. Lazzarotto,[1] P. Lipari,[14,15] F. Longo,[8,9] F. Fuschino,[5] M. Marisaldi,[5] S. Mereghetti,[7] E. Morelli,[5] E. Moretti,[8,9] A. Morselli,[4] L. Pacciani,[1] F. Perotti,[7] G. Piano,[1,4] P. Picozza,[1,4] M. Prest,[17] M. Rapisarda,[6] A. Rappoldi,[10] A. Rubini,[1] S. Sabatini,[1,4] P. Soffitta,[1] E. Vallazza,[9] A. Zambra,[3,7] D. Zanello,[14,15] F. Lucarelli,[19] P. Santolamazza,[19] P. Giommi,[19] L. Salotti,[20] G. F. Bignami[25]

The well-known Crab Nebula is at the center of the SN1054 supernova remnant. It consists of a rotationally powered pulsar interacting with a surrounding nebula through a relativistic particle wind. The emissions originating from the pulsar and nebula have been considered to be essentially stable. Here, we report the detection of strong gamma-ray (100 mega–electron volts to 10 giga–electron volts) flares observed by the AGILE satellite in September 2010 and October 2007. In both cases, the total gamma-ray flux increased by a factor of three compared with the non-flaring flux. The flare luminosity and short time scale favor an origin near the pulsar, and we discuss Chandra Observatory x-ray and Hubble Space Telescope optical follow-up observations of the nebula. Our observations challenge standard models of nebular emission and require power-law acceleration by shock-driven plasma wave turbulence within an approximately 1-day time scale.

The Crab Nebula (*1*) is a relic of a stellar explosion recorded by Chinese astronomers in 1054 A.D. It is located at a distance of 2 kpc from Earth and is energized by a powerful pulsar of spindown luminosity $L_{PSR} = 5 \times 10^{38}$ erg s^{-1} and spin period $P = 33$ ms (*2*–*4*). Optical and x-ray images of the inner nebula show (*1*, *5*–*7*) features such as "wisps" (composing a torus-shaped structure), "knots," and the "anvil" [positioned along the South-East "jet" originating from the pulsar and aligned with its rotation axis (*6*)]. Wisps, some of the knots, and the anvil are known to brighten and fade over weeks or months (*6*, *8*). The Crab Nebula x-ray continuum and gamma rays up to ~100 MeV energies are modeled by means of synchrotron radiation and emission from giga- to teraelectron volt energies as inverse Compton radiation by accelerated electrons scattering cosmic microwave background (CMB) and nebular photons (*9*–*12*).

The AGILE (Astro–rivelatore Gamma a Immagini Leggero) satellite (*13*) observed the Crab Nebula several times both in pointing mode from mid-2007 to mid-2009 and in spinning mode starting in November 2009 [supporting online material (SOM) text]. The AGILE instrument (*13*)

[1]Istituto Nazionale di Astrofisica–Istituto di Astrofisica Spaziale e Fisica Cosmica (INAF-IASF) Roma, via del Fosso del Cavaliere 100, 00133 Roma, Italy. [2]Dipartimento di Fisica, Università degli Studi di Roma "Tor Vergata," via della Ricerca Scientifica 1, 00133 Roma, Italy. [3]Consorzio Interuniversitario Fisica Spaziale (CIFS), villa Gualino, v.le Settimio Severo 63, 10133 Torino, Italy. [4]Istituto Nazionale di Fisica Nucleare (INFN) Roma Tor Vergata, via della Ricerca Scientifica 1, 00133 Roma, Italy. [5]INAF-IASF Bologna, via Gobetti 101, 40129 Bologna, Italy. [6]Ente per le Nuove tecnologie, l'Energia e l'Ambiente (ENEA) Frascati, via Enrico Fermi 45, 00044 Frascati(RM), Italy. [7]INAF-IASF Milano, via E. Bassini 15, 20133 Milano, Italy. [8]Dipartimento di Fisica, Università di Trieste, via A. Valerio 2, 34127 Trieste, Italy. [9]INFN Trieste, Padriciano 99, 34012 Trieste, Italy. [10]INFN Pavia, via Bassi 6, 27100 Pavia, Italy. [11]Dipartimento di Fisica Generale, Università degli Studi di Torino, via P. Giuria 1, 10125 Torino, Italy. [12]ENEA Bologna, via don Fiammelli 2, 40128 Bologna, Italy. [13]Space Research Institute, Russian Academy of Sciences, 84/32 Profsoyuznaya Street, 117997 Moscow, Russia. [14]INFN Roma 1, p.le Aldo Moro 2, 00185 Roma, Italy. [15]Dipartimento di Fisica, Università degli Studi di Roma "La Sapienza," p.le Aldo Moro 2, 00185 Roma, Italy. [16]INAF Osservatorio Astronomico di Cagliari, Poggio dei Pini, 09012 Capoterra, Italy. [17]Dipartimento di Fisica, Università degli Studi dell' Insubria, via Valleggio 11, 22100, Como, Italy. [18]INAF-IASF Palermo, via La Malfa 153, 90146 Palermo, Italy. [19]Agenzia Spatiale Italiana (ASI) Science Data Center, European Space Agency (ESA) Centre for Earth Observation (ESRIN), 00044 Frascati, Italy. [20]ASI, viale Liegi 26, Roma, Italy. [21]NASA, Marshall Space Flight Center, Huntsville, AL 35812, USA. [22]Institut fuer Experimentalphysik, University of Hamburg, Hamburg 22761, Germany. [23]Integral Science Data Centre, University of Geneva, Chemin d'Ecogia 16, CH-1290 Versoix, Switzerland. [24]Department of Physics, University of Alberta, Edmonton, Alberta T6G 2G7, Canada. [25]Istituto Universitario di Studi Superiori (IUSS), I-27100 Pavia, Italy.

*To whom correspondence should be addressed. E-mail: pi.agile@iasf-roma.inaf.it